Q. J. R. Meteorol. Soc. (1999), **125**, pp. 1997–2018

The role of sound waves in sea-breeze initiation

By A. B. C. TIJM* and A. J. VAN DELDEN
Institute for Marine and Atmospheric Research Utrecht, The Netherlands

(Received 16 March 1998; revised 29 June 1998)

SUMMARY

The dynamics of the pressure distribution associated with the sea-breeze circulation is investigated. Analysis of hourly observations of surface pressure reveals that, on a typical sea-breeze day, large surface-pressure falls are recorded very far inland. Using a linear numerical model we show that this can only be understood when sound waves are taken into account. Sound waves are excited when air in the boundary layer over land expands due to diabatic heating. The numerical study reveals that vertically travelling sound waves induce a pressure increase through the entire atmosphere above the heated layer within a few minutes, while horizontally travelling sound waves induce a surface-pressure decrease over land and a surface-pressure increase over sea, with the resulting horizontal surface-pressure gradient initiating the sea breeze. Because the signal travels inland at the speed of sound (about 300 m s^{-1}), points at a distance of more than 1000 km from the coast experience a surface-pressure decrease within an hour after the initiation of diabatic heating over land. The pressure decrease near the earth's surface over land, as well as the pressure increase aloft, is in accord with the observations at mountain stations and the analyses of the observed daytime surface-pressure changes in summer over the continent and adjacent seas. The implications of these findings for hydrostatic modelling of sea breezes are investigated. It appears that after one hour the hydrostatic sea breeze is 10% stronger than the non-hydrostatic sea breeze, while the hydrostatic return current is about 20% weaker.

KEYWORDS: Non-hydrostatic model Sea-breeze observations Sound waves

1. INTRODUCTION

Despite the fact that we know a lot about the sea breeze, there are still different qualitative explanations of the development of the pressure gradients that initiate the sea breeze. Three such explanations can be found in meteorological textbooks.

The first explanation, which we refer to as the 'upward' theory (see Fig. 1(a)), has been described by Koschmieder (1933), Defant (1951), Willet and Sanders (1959), Atkinson (1981) and Pielke (1984). On days with clear and calm weather, the air over land is heated more rapidly than over sea. Therefore the air in the boundary layer above land is warmer than the air above the sea. Assuming hydrostatic conditions, the vertical pressure gradients are larger over sea than over land. If we assume that the pressure at the surface remains the same at first, we see that the pressure above the surface is higher over land than over sea. The horizontal pressure gradient now present, causes a flow from the land towards the sea. The mass divergence over the land and the mass convergence over the sea cause the pressure at the surface to fall over land and to rise over sea. This initiates the sea breeze near the earth's surface.

The second explanation, which we call the 'sideways' theory (see Fig. 1(b)), has been described by Simpson (1994). In this explanation, a *level of no pressure change* is assumed to exist at a certain height above the convective boundary layer, so that the sideways expansion of each column of air over land produces changes in pressure which, according to Simpson, are transmitted sideways with the speed of sound. The resulting pressure difference at low levels is responsible for the onset of the sea breeze. The pressure decrease over land should initially be the same everywhere if the land surface is homogeneous and is heated uniformly. When the sea breeze sets in, the surface pressure will fall less rapidly near the coast than farther inland due to advection of cool sea air. Figure 2, which shows the average surface-pressure changes around noon in June over Europe, supports this explanation. Note the large negative pressure tendencies over central Europe, about 1000 km from the coast.

* Corresponding author, present address: KNMI, Postbus 201, 3730 AE De Bilt, The Netherlands.

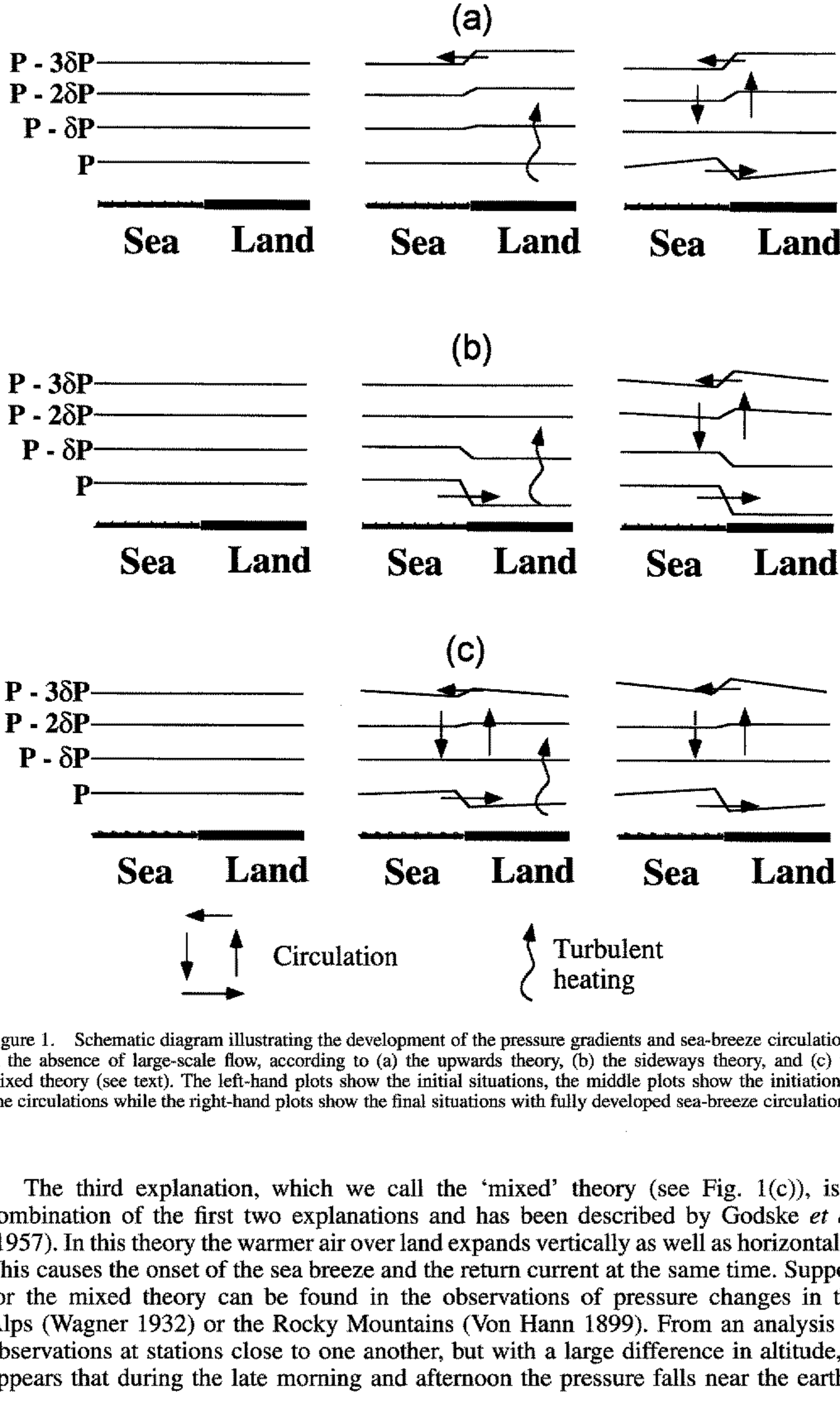

Figure 1. Schematic diagram illustrating the development of the pressure gradients and sea-breeze circulations, in the absence of large-scale flow, according to (a) the upwards theory, (b) the sideways theory, and (c) the mixed theory (see text). The left-hand plots show the initial situations, the middle plots show the initiation of the circulations while the right-hand plots show the final situations with fully developed sea-breeze circulations.

The third explanation, which we call the 'mixed' theory (see Fig. 1(c)), is a combination of the first two explanations and has been described by Godske *et al.* (1957). In this theory the warmer air over land expands vertically as well as horizontally. This causes the onset of the sea breeze and the return current at the same time. Support for the mixed theory can be found in the observations of pressure changes in the Alps (Wagner 1932) or the Rocky Mountains (Von Hann 1899). From an analysis of observations at stations close to one another, but with a large difference in altitude, it appears that during the late morning and afternoon the pressure falls near the earth's

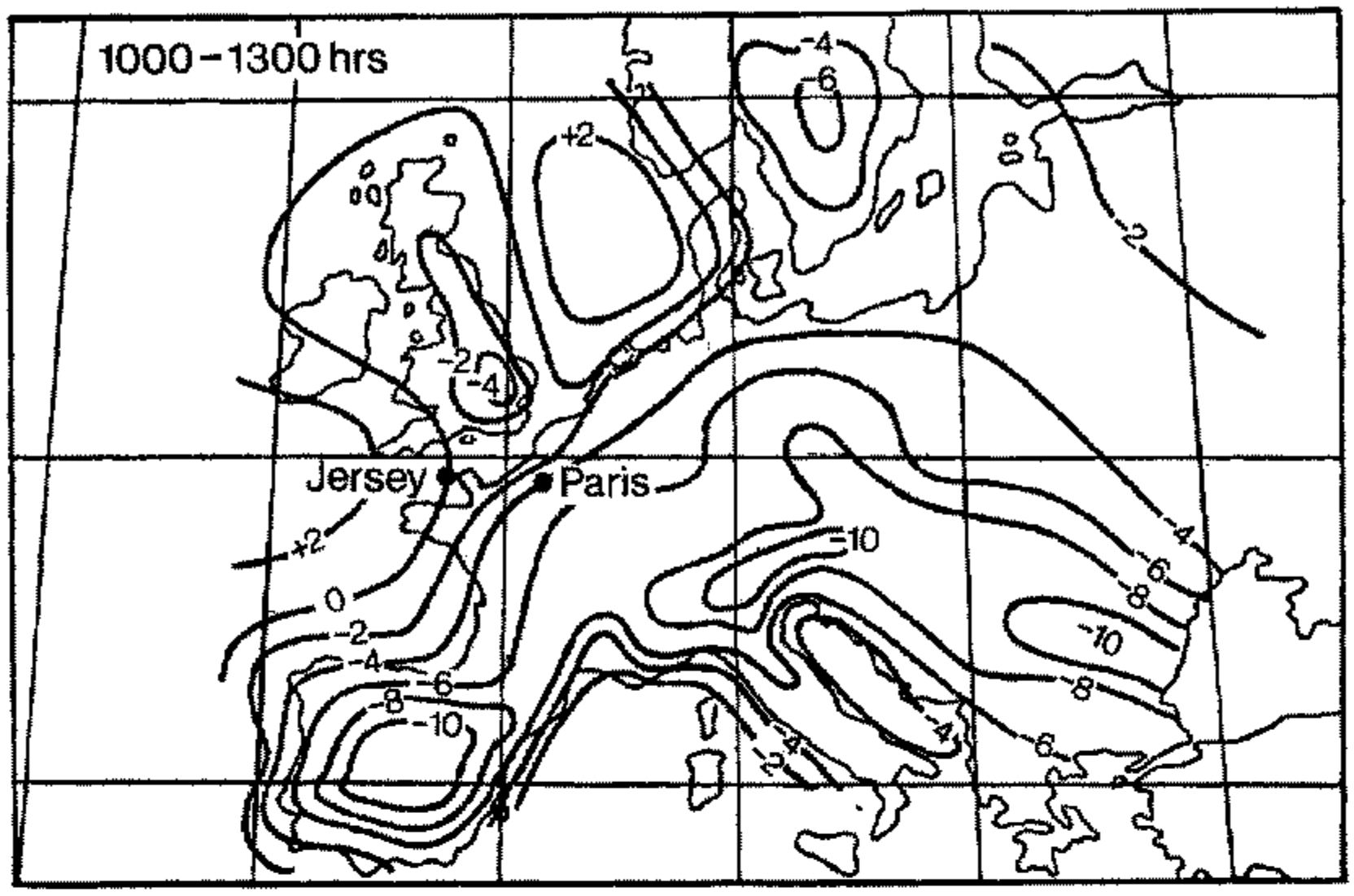

Figure 2. Surface pressure changes (tenths of hPa) in Europe between 1000 and 1300 UTC in June (from Simpson 1994).

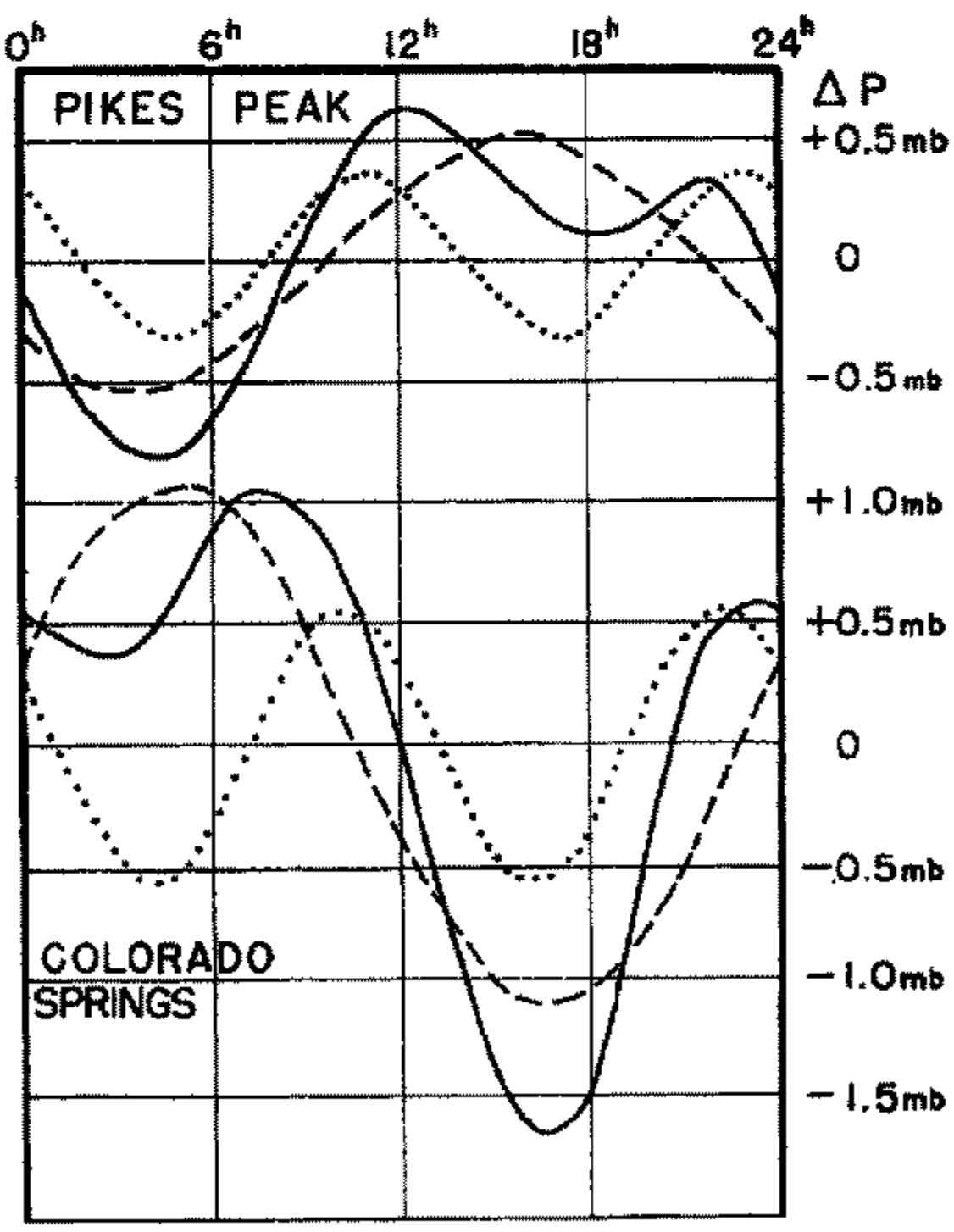

Figure 3. Harmonic analysis of the diurnal and semi-diurnal pressure waves during summer at Pikes Peak (altitude 4308 m, upper curves) and at Colorado Springs (altitude 1856 m, lower curves) (data from Von Hann (1899), figure from Godske *et al.* (1957)). The solid line represents the total variation, the dashed line is the diurnal component and the dotted line is the semi-diurnal component of the pressure changes.

surface while it rises aloft (see Fig. 3 and the analysis by Godske *et al.* (1957)). The level of no pressure change was located at about 800 m above the earth's surface.

In several textbooks the Bjerknes circulation theorem is used to explain sea breezes (e.g. Bjerknes *et al.* 1933; Brunt 1939; Hess 1959; Atkinson 1981; Holton 1992). We do not list this as a separate explanation because it only states that there will be a circulation when there is baroclinicity and when forces are not in balance. It does not explain the origin of the pressure differences near the earth's surface.

In all these three explanations the pressure field is deduced from the temperature field using the hydrostatic equation, together with a boundary condition on the pressure. However, in the mixed theory, as well as in the sideways theory, specifying a realistic boundary condition is a serious problem because it is actually not possible to fix the level of no pressure change, as in the upward theory. This is presumably the reason for the greater popularity of the upward theory.

Nevertheless, many hydrostatic numerical models that are used to investigate the structure, dynamics and characteristic features of sea breezes (e.g. Estoque 1962; Pielke 1974; Tijm *et al.* 1999) are most consistent with the sideways theory. The boundary condition used in these models is a fixed pressure at the top of the model domain (a rigid lid or a material surface). The pressure at the other levels is calculated from the vertical temperature profile by integrating the hydrostatic equation from the model top *downwards*. Thus, as in the sideways theory, changes in the vertical temperature profile are the direct cause for changes in the surface pressure. This implies an instantaneous loss of mass over land as a result of diabatic heating. The mixed theory, which intuitively appears to be the best explanation for sea-breeze initiation, cannot be implemented in a hydrostatic model because of the impossibility of specifying a boundary condition on the pressure. Implementing the upward theory in a hydrostatic model requires an extra prognostic equation for the pressure at the earth's surface. The pressure at the other levels is then calculated by integrating the hydrostatic equation upwards (e.g. Physick 1976; Anthes and Warner 1978). This results in the occurrence of high-speed Lamb waves limiting the possible time step, or minimum grid distance, of the model. Making a hydrostatic sea-breeze model consistent with the sideways theory, implies living with the fact that there is no compensation for the loss of mass over land in the model, since the mechanism taking care of the transport of mass towards the sea, i.e. the sound wave, is neglected. The importance of this error will be investigated in this paper.

The chain of interactions forming a sound wave as a result of diabatic heating has been described by Scorer (1997), as follows. When a stagnant body of air is heated its pressure is increased, while the pressure in the surroundings is unaltered. The heated air expands, pushing the surrounding air outwards. The positive pressure perturbation thus spreads outwards, taking the form of a sound wave with a phase speed of approximately 300 m s^{-1}. Nicholls and Pielke (1994a and b) refer to the type of sound wave forced by diabatic heating as a *thermal compression wave* to distinguish it from the more commonly studied mechanically forced high-frequency sound wave. Here, we adhere to the term 'sound wave'.

One way to check which theory comes closest to the truth is to look at the observed surface-pressure changes during days when strong heating of the boundary layer gives rise to sea breezes. If the upward theory is correct the largest changes in surface pressure would be recorded in the vicinity of the coast, where there is divergence of air towards the sea. Far inland there would initially be no change in surface pressure, because the divergence and convergence would first take place in the vicinity of the coast. In the mixed theory, the surface pressure decreases over land as a direct reaction to the daytime heating of the boundary layer, while in the upward theory the surface pressure

decreases over land only as a consequence of mass divergence aloft. In the mixed theory the surface pressure over land will also decrease as a consequence of the heating, but less rapidly than in the sideways theory, i.e. not in accordance with the amount of heat added to the boundary layer.

In any case all three qualitative explanations appear incomplete, principally because the mechanism which creates the pressure differences that initiate the sea breeze, i.e. the sound wave, is not (or is barely) mentioned. A hydrostatic model, therefore, also misrepresents the onset of the sea breeze. Of course, the question is: how serious is this quantitatively? We address this question in this paper. We first analyse the observed surface-pressure changes on sea-breeze days in the Netherlands. The observational area is described in section 2. The synoptic observations are discussed in section 3. In section 4 the important role played by sound waves in determining the spreading of the pressure perturbation induced by differential heating is investigated with the aid of a two- dimensional linear model. We conclude with a discussion of the implication of the results for hydrostatic numerical modelling of sea breezes and other thermally generated circulations.

2. Observational area

The Royal Netherlands Meteorological Institute operates a dense network of synoptic stations (see Fig. 4) at which routine measurements are performed on a hourly basis. The highest density of these stations is found near the western coastline, which is nearly straight. To the south-west the coastline is very irregular, while to the north the circulations can be influenced by Lake IJssel. Orography is almost absent in the first 50 km from the coast, apart from a strip of sand dunes near the coast. The latter have an average height of 10 to 20 m, with the highest peaks up to 57 m in the north. At about 90 km inland hills with a maximum height of 106 m are present, while orography exceeding 200 m in height is situated more than 150 km inland. This makes the Netherlands a very suitable location to perform sea-breeze studies.

Of the ten stations used in this study, four are situated over sea. Station 239 (not in Fig. 4) lies about 150 km north-north-east of station 550. Stations 553 and 554 represent the region near the coast. Of the first two stations on the land, station 330 lies at the coast, while station 210 is situated about 3 km inland. Stations 344 and 260 represent the region a short distance inland, while stations 370 and 380 lie farthest inland (more than 100 km).

3. Synoptic observations

With the aid of synoptic observations (of the wind, the temperature and the surface pressure reduced to sea level) on 53 days with sea breezes at the west coast of the Netherlands during the years 1994 and 1995, we try to assess the validity of the three theories for the initiation of sea breezes. A day was considered as a sea-breeze day in this study on the basis of the following criteria: the average winds between 06 and 10 UTC at the land-based stations were directed offshore; the average winds at stations 330 and 210 between 13 and 16 UTC were directed onshore; the maximum (positive) temperature difference between the air over land and over sea exceeded 5°C. Days with large-scale frontal passages that met these criteria were removed manually.

All days included in this study occurred between April and August, with most cases in May and June (the times of sunrise and sunset between April and August do not vary by more than about one hour). The data for these cases were averaged hour by hour

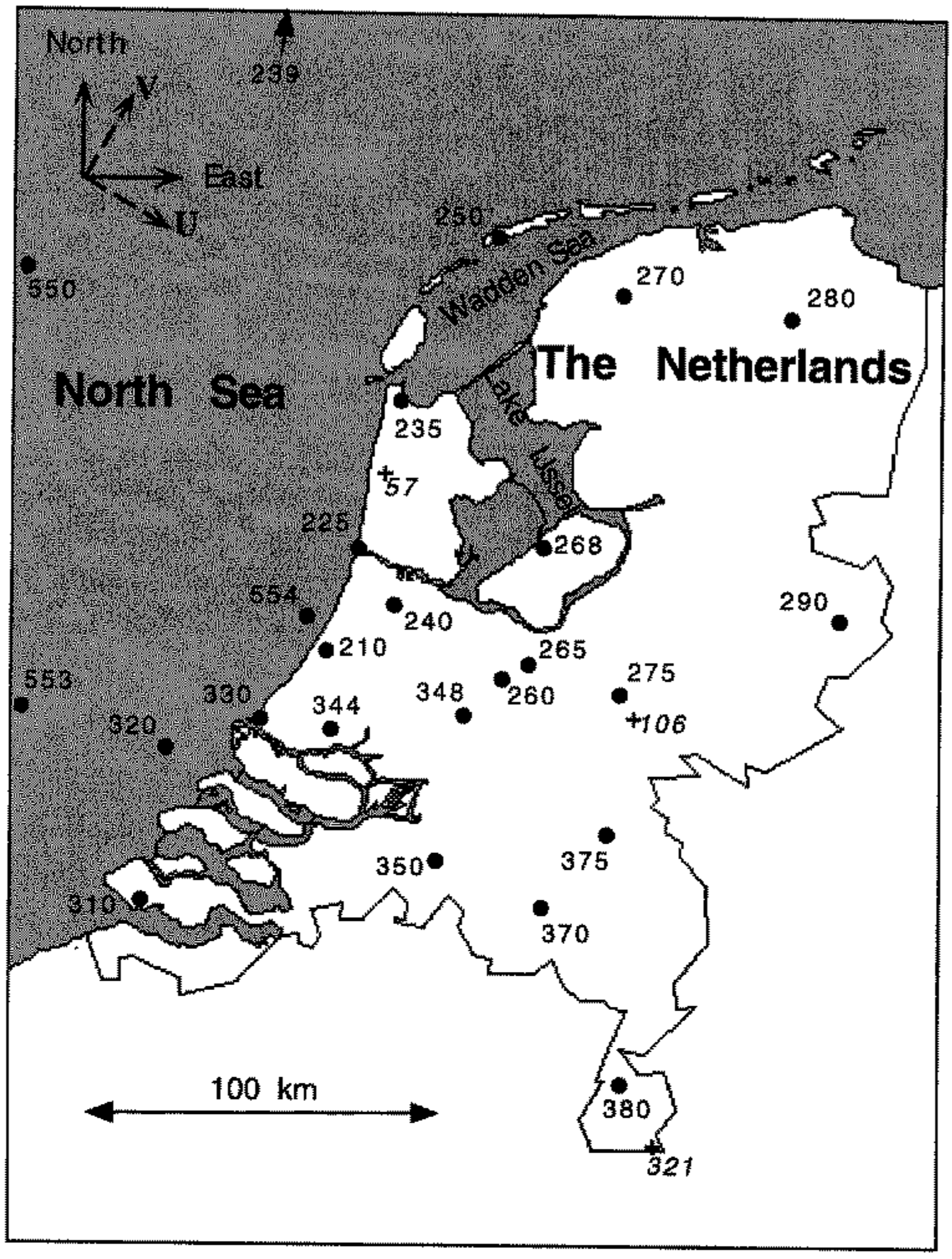

Figure 4. Map indicating the locations of observating stations operated by the Royal Netherlands Meteorological Institute, together with some spot surface elevation values (crosses and heights in m).

resulting in an average daily cycle of the wind components, the temperature and the surface pressure at the stations used in this study.

The synoptic measurements of wind and temperature were used to determine the time of onset of the sea breeze at the different stations. The sea breeze first sets in at stations 554 and 330 (Fig. 5) where the component of the wind blowing perpendicular to the coast (the U-component) becomes positive at 09 UTC. This happens about one hour later at station 210 (positioned 3 km inland). After that it takes about three hours for the sea breezes to reach station 344 (about 20 km inland).

The onset of the sea breeze can also be seen very clearly in the wind component blowing parallel to the coast (the V-component). After the U-component has become positive, the V-component becomes increasingly negative due to the Coriolis turning of the wind. The daily cycle of the temperature also shows clearly the influence of the sea breeze. The daily cycle is almost absent in the data from stations at sea far from the coast. Station 554 shows some warming during the day, especially in the morning. After the onset of the sea breeze at this station the temperature still rises a little, where a slight drop in temperature should be expected because the advection of warm land air

has stopped; this rise must be caused by subsidence. The onset of the sea breeze is very clear at station 330, where the rise of the temperature stops abruptly at the moment of onset of the sea breeze. This happens later further inland.

Figure 6 shows clearly the strong influence of the semi-diurnal tide. A second important phenomenon is the tendency of the surface pressure to be lower at the end of the day than at the start; this effect is weak over sea and becomes stronger farther inland. It can probably be attributed to the formation of a thermal low over the continent during days with strong heating of the atmosphere.

Because we are interested in the pressure perturbations caused by the differential heating and the sea breeze, the overshadowing effects of the atmospheric tide and the large-scale pressure tendency have to be removed. We achieve this by using the hour-to-hour change of the surface-pressure perturbation relative to the average hour-to-hour change of the surface-pressure perturbation at all stations. If the sideways theory is valid, the surface pressure will decrease with increasing average boundary-layer temperature. The largest fall in pressure will occur in the area not influenced by the sea breeze, that is far inland. If, on the other hand, the the upward theory is valid the largest changes in the surface pressure should occur in the area near the sea-breeze front.

The hour-to-hour pressure changes (Fig. 7) show the effect of the sea breeze. For the sake of clarity the data have been smoothed (averaged over three points). One has to bear in mind that these pressure changes are relative to the spatially averaged pressure changes, and so the absolute pressure changes are probably different. During the night there is little difference between the stations situated on land or at sea. The pressure tends to fall slightly at sea, while over land we see the opposite. During the first few hours after sunrise (between 04 and 06 UTC) not much happens. However, after 06 UTC large differences develop between the pressure changes over land and over sea. The relative average-pressure falls are strongest far inland, while the opposite is the case over sea. Around 11 UTC (about the time of the strongest insolation) the difference in pressure change is about 0.25 hPa h^{-1} (i.e. the difference between the pressures at stations 239 and 380). After 11 UTC the differences become smaller while after 15 UTC we see the relative pressure change becoming negative over sea and positive over land.

The daily cycle of the surface-pressure changes is clearly a function of the distance to the coast. During the daytime, the largest rises and falls of the surface pressure are recorded at the stations farthest from the coastline. The 10 stations used in this study can be divided into 4 groups, each with a different reaction of the surface pressure to the influence of the heating of the boundary layer and the sea breeze. The first group consists of stations 239 and 550, the stations at sea farthest from the coast. These show the largest relative surface-pressure rise during daytime. From the observations of the wind components and the temperature it is clear that these stations are not influenced by the sea breeze. The second group includes stations 553 and 554 located at about 50 km and 5 km from the coast, respectively, but still at sea. These stations are influenced by the sea breezes and show smaller relative surface-pressure rises than the first group. This is probably caused by the advection of warmer air aloft giving rise to a decrease in the hydrostatic surface pressure. The third group consists of stations 330 and 210; these lie on land but near the coastline. In the early morning the relative surface-pressure change is negative (as at the other land stations) but, after the onset of the sea breeze, the relative surface-pressure change becomes positive (as at the sea stations). The positive relative surface-pressure change is caused by the advection of cool air by the sea breeze compensating for the turbulent heating of the boundary layer. Group four consists of stations 344, 260, 370 and 380 situated about 20, 50, 100 and 150 km inland, respectively. The relative surface-pressure change at these stations remains negative

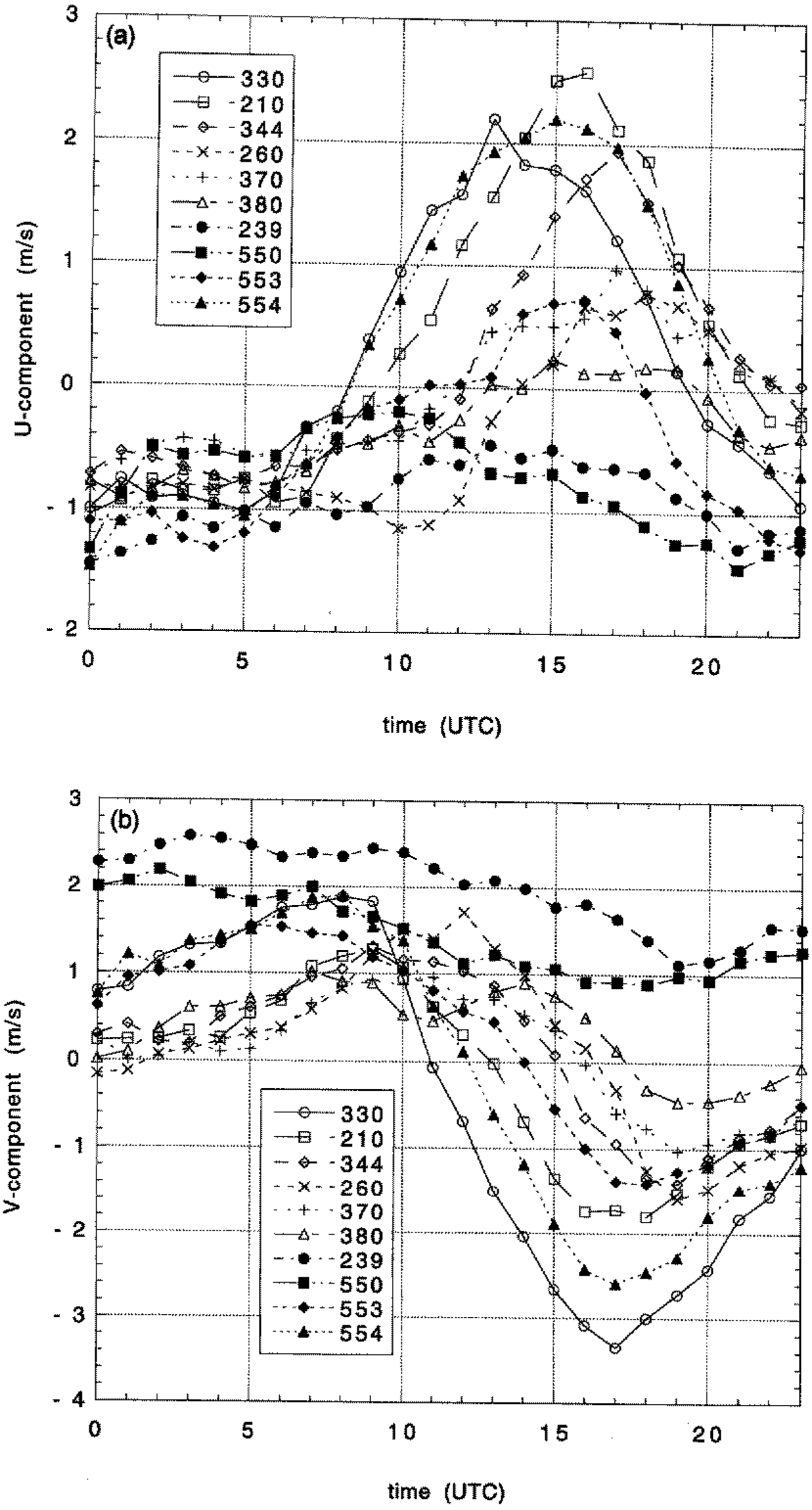

Figure 5. The daily cycle, averaged over 53 sea-breeze days, of (a) the wind component perpendicular to the coast, (b) the wind component parallel to the coast, and (c) the 2 m temperature. The numbers in the key refer to observing stations illustrated in Fig. 4.

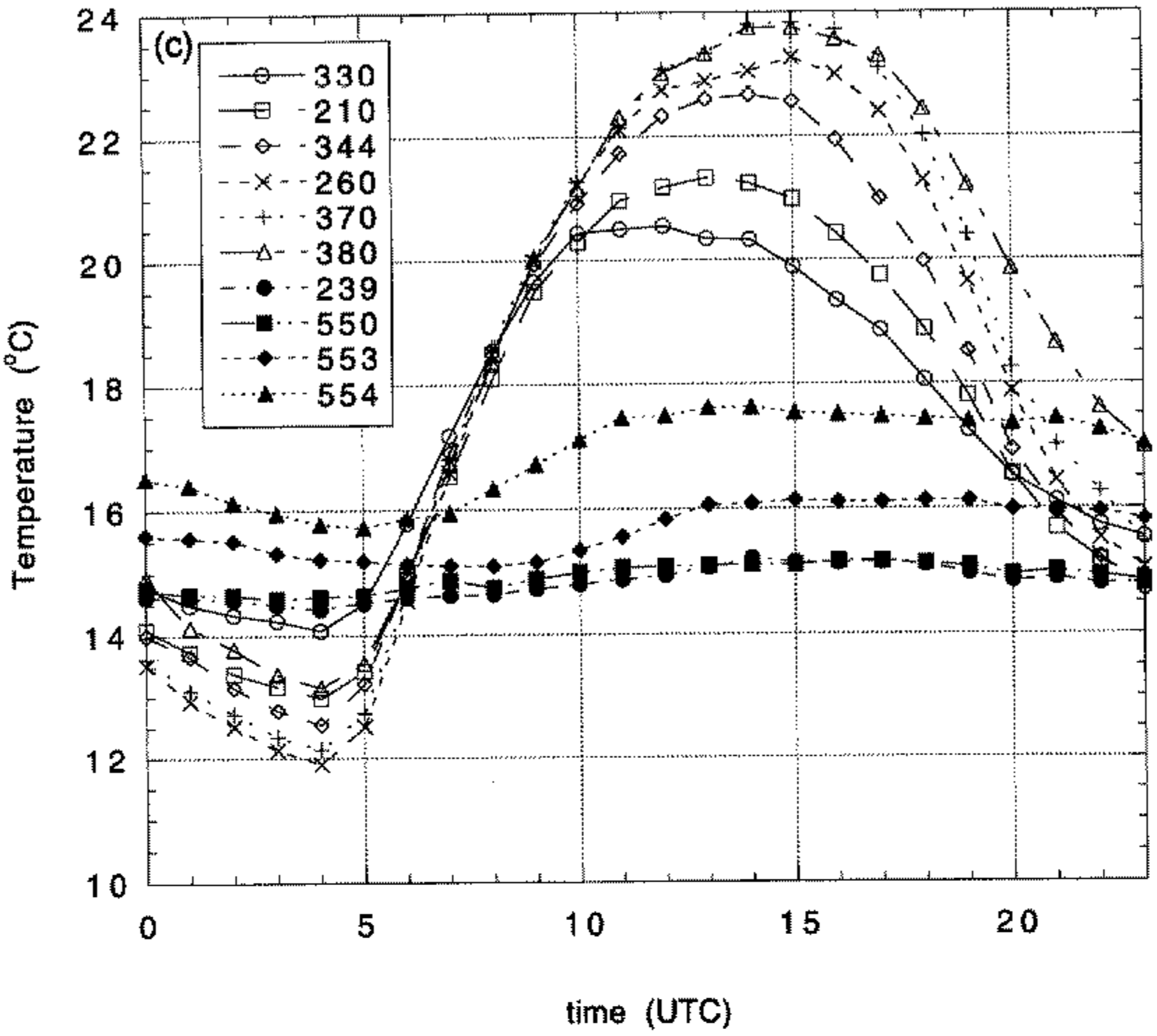

Figure 5. Continued.

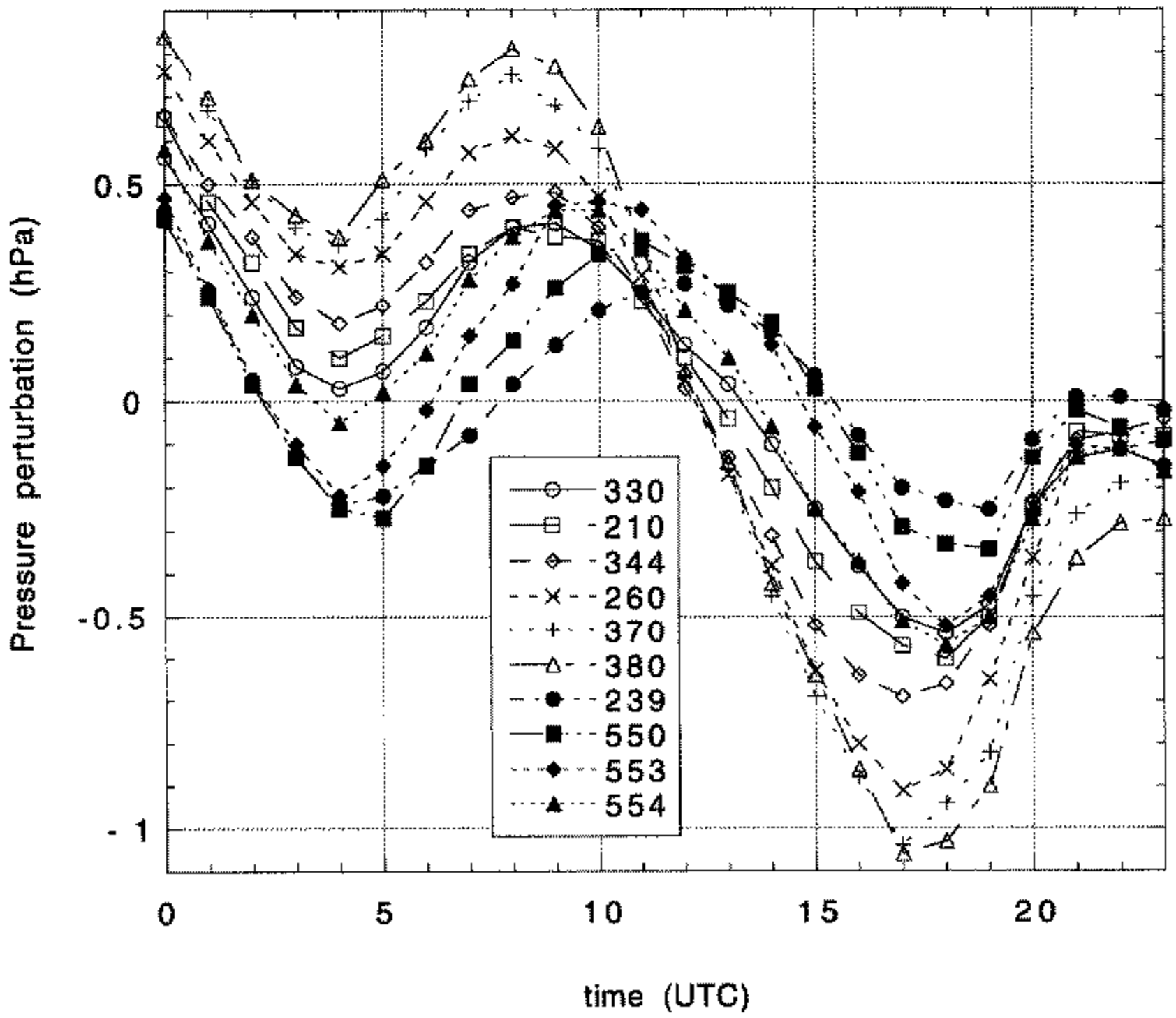

Figure 6. The daily cycle, averaged over 53 sea-breeze days, of the surface pressure perturbation (hPa) at 10 stations. The numbers in the key refer to observing stations illustrated in Fig. 4.

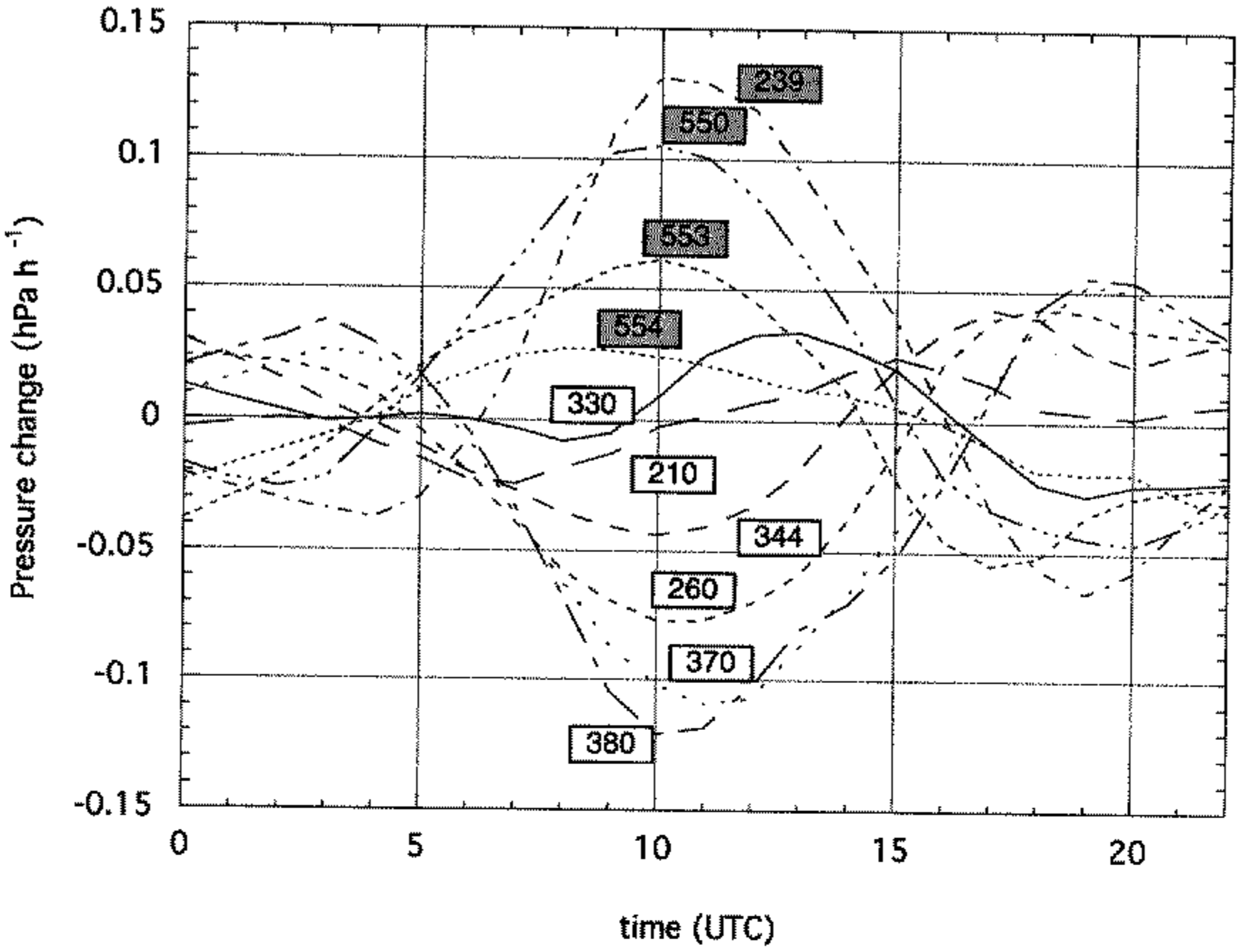

Figure 7. The daily cycle, averaged over 53 sea-breeze days, of the relative hour-to-hour pressure changes (hPa h^{-1}). The numbers in the boxes refer to observing stations illustrated in Fig. 4 (stations at sea are shaded).

during the daytime, with the largest negative value being found at the station farthest inland.

When the observed average daily cycle of the pressure changes are compared with theory, it seems that the upward theory must be rejected. In the upward theory the largest pressure fall should occur near the coast before the onset of the sea breeze, while far inland the pressure should remain constant. In this study, however, it is clear that after 07 UTC the largest pressure falls take place far inland. This result agrees with the results shown earlier in Fig. 2.

4. SEA-BREEZE INITIATION IN A LINEAR NUMERICAL MODEL

In this study we use a two-dimensional linearized non-hydrostatic model to calculate the pressure differences caused by differential heating of the air. Sound waves are included in the model and the following equations are used:

$$\frac{\partial \Theta'}{\partial t} = \frac{1}{\Pi_0} J - w \frac{\partial \Theta_0}{\partial z}, \quad \text{with} \quad \Pi_0 = c_p \left(\frac{p_0}{p_{\text{ref}}} \right)^{\frac{R}{c_p}}, \tag{1}$$

$$\frac{c_v}{R\Pi_0} \frac{\partial \Pi'}{\partial t} = \frac{c_v}{R\Pi_0} \frac{g}{\Theta_0} w - \frac{\partial u}{\partial x} - \frac{\partial w}{\partial z} + \frac{1}{\Pi_0 \Theta_0} J, \tag{2}$$

$$\frac{\partial u}{\partial t} = -\Theta_0 \frac{\partial \Pi'}{\partial x}, \tag{3}$$

$$\frac{\partial w}{\partial t} = -\Theta_0 \frac{\partial \Pi'}{\partial z} + g \frac{\Theta'}{\Theta_0}, \tag{4}$$

where Π is the Exner function ($=c_p(p/p_{\text{ref}})^{R/c_p}$), p the pressure, p_{ref} the reference pressure (=1000 hPa), Θ the potential temperature, u the horizontal wind component, w the vertical wind component, J the amount of heat added per unit mass, c_v the specific heat of dry air at constant volume, c_p the specific heat of dry air at constant pressure, R the gas constant for dry air and g the acceleration due to gravity at sea level. These equations are linearized around a basic state $(u, w, \Theta, \Pi) \equiv (0, 0, \Theta_0(z), \Pi_0(z))$ which is in hydrostatic equilibrium, $\partial\Pi_0/\partial z = g/\Theta_0$ (Van Delden 1992). The primes denote the perturbation from the basic state, except for u and w which are zero initially. Because we are interested in the onset of the sea breeze, the linearization is reasonably accurate. Note that in Eqs. (1) to (4) the Coriolis force is neglected because it is of little importance for the relatively short model runs we perform (less than or equal to three hours), and that friction and turbulence are also neglected.

Theoretically, sound-waves and buoyancy-waves are solutions of the Eqs. (1) to (4), and are therefore part of our numerical model. When we substitute wave-like solutions in these equations and assume that $\Theta_0 \approx \Theta_m \equiv$ constant, $\Pi_0 \approx \Pi_m \equiv$ constant and $d\Theta_0/dz = 0$, we find the following dispersion relation for sound waves:

$$\omega^2 = c^2(\alpha^2 + \gamma^2) + \frac{1}{4}\frac{g^2}{c^2}, \tag{5}$$

where ω is the frequency, α is the horizontal wave number, γ is the vertical wave number, and c is the speed of sound ($c^2 = R\Pi_m\Theta_m/c_v$). The dispersion relation for the buoyancy waves can be found by assuming that $\partial\Theta_0/\partial z \equiv$ constant and taking the limit $c \to \infty$:

$$\omega^2 = \frac{\alpha^2 N^2}{\alpha^2 + \gamma^2} = N^2 \sin^2\phi. \tag{6}$$

Here, N^2 is the Brunt–Väisällä frequency $(g/\Theta_m)(\partial\Theta_0/\partial z)$ and ϕ is the angle between the phase-propagation direction of the buoyancy wave and the z-axis.

Equations (1) to (4) are solved on a staggered grid with a horizontal grid-length of 5 km for a short run of 200 s, and 100 km for a long run of 3 h. Towards the lateral boundaries the grid-length is increased to prevent interference of reflections from these boundaries with the solution in the centre of the domain. In the vertical direction the grid-length is 100 m near the surface, and increases with height. There are 61 model points in the horizontal direction and 60 in the vertical direction. The horizontal domain of equally spaced inner grid-points extends from 100 km out to sea to 100 km over land for the short run, and from 2000 km over the sea to 2000 km over the land for the long run. The vertical domain extends from the surface up to a height of 127 km.

Similar experiments have already been performed by Nicholls and Pielke (1994a and b). However, these authors used a much coarser grid ($\Delta x = 50$ km and $\Delta z = 1$ km) and only one grid point in the vertical direction was heated. In our study, more details of the vertical structure of the atmosphere's reaction to the applied heating are revealed through the fine resolution ($\Delta z \sim 100$ to 200 m in the heated layer). Also, we focus on the sea breeze initiation while Nicholls and Pielke focused on the energy transfer.

Because fast-moving sound waves are a solution to the Eqs. (1) to (4) a small time step of 0.1 s must be taken. The equations are discretized using the leap-frog scheme for the time derivatives and central differences for the other terms.

We impose zero gradients for all variables at the lateral boundaries and fixed (initial) gradients at the top boundary. At the surface, the horizontal and vertical velocity are

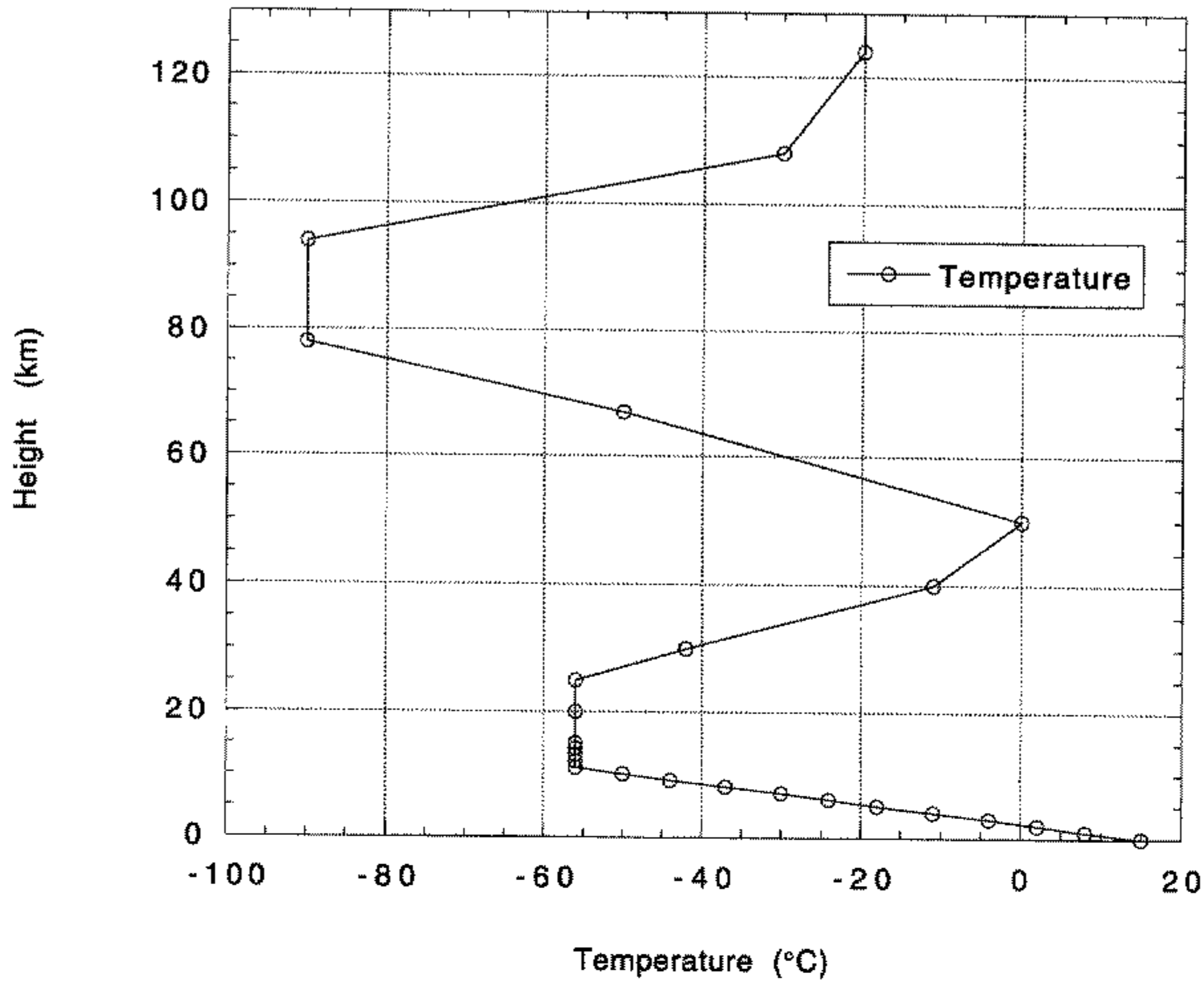

Figure 8. The initial vertical temperature profile used in the model.

taken to be zero. The initial vertical temperature profile up to a height of about 30 km is defined from US Standard Atmosphere data (US Government Printing Office 1976) (see Fig. 8). From 30 km up to 100 km we use the average temperature profile from Chapman and Lindzen (1970), and above this height we impose a uniform temperature of 253 K. The model is continuously forced by heating of the layer from the surface up to 2000 m over land. The forcing decreases linearly with height to prevent the temperature profile from becoming neutral or unstable. The total added heat corresponds to a surface heat flux of about 275 W m^{-2} and an average heating of the 2000 m thick layer of about 0.5 K h^{-1}.

(*a*) *Short model run*

Next we discuss the chain of events following the initiation of the heating over land. To investigate the initial reaction of the atmosphere to the forcing described above, Eqs. (1) to (4) were integrated for 200 s on a 5 km grid. The increasing temperature in the layer from the surface to 2000 m initially causes a pressure rise over land ($\partial \Pi'/\partial t \sim \mathrm{d}Q/\mathrm{d}t$), which is indicated by the positive Exner-function perturbation over land in the first seconds (Fig. 9(d)). This pressure rise (which is a deviation from hydrostatic equilibrium) causes pressure gradients at the top and the side (coast) of the warming layer, leading to accelerations in the horizontal direction near the coast and the vertical direction at the top of the warming layer over land. The vertical velocities over land are stronger far inland than near the coast (compare Figs. 9(b) and (c)). This is due to the fact that the acceleration near the coast also takes place in the horizontal direction, leading to horizontal divergence and decreasing pressure gradients.

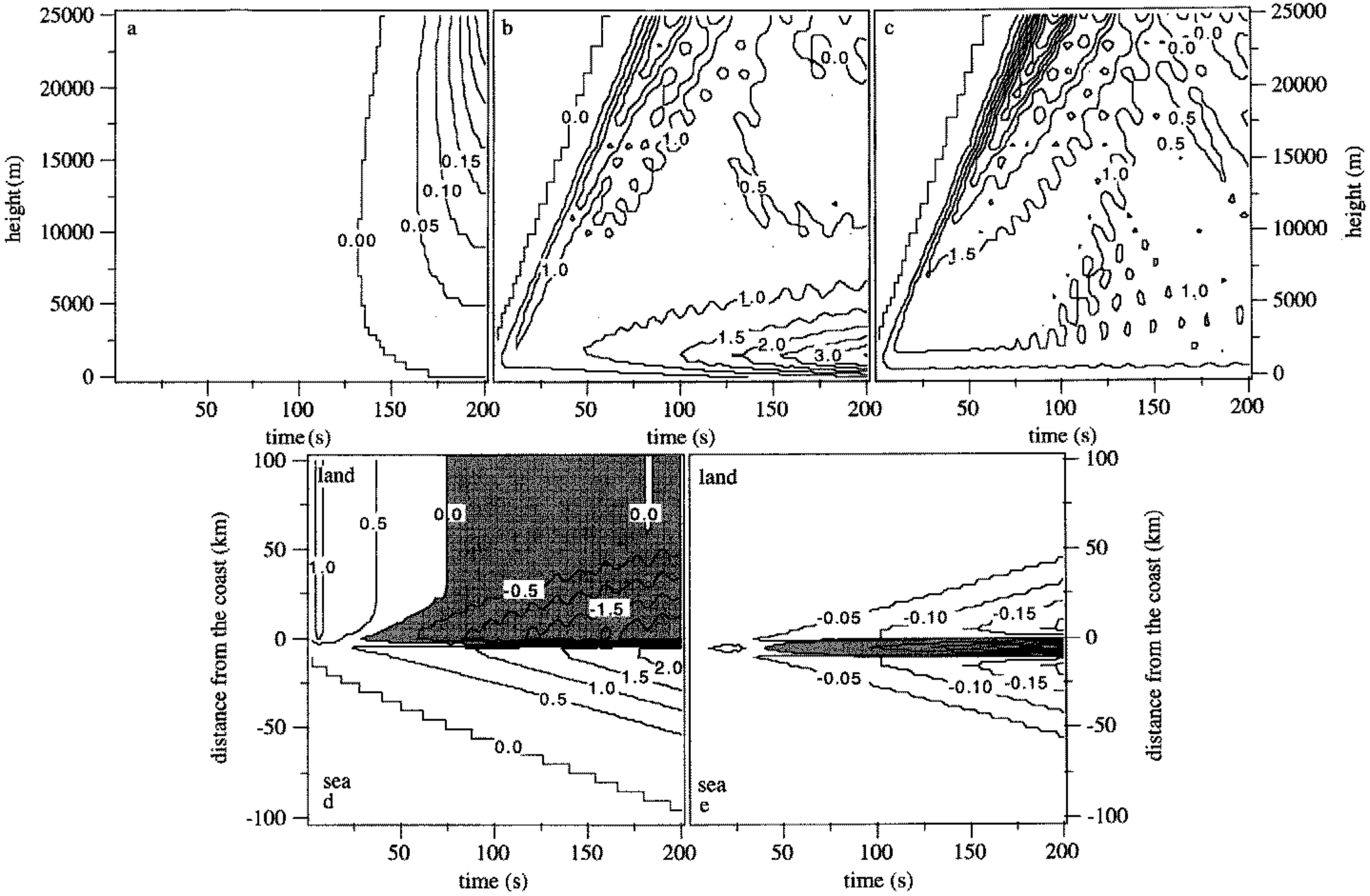

Figure 9. The vertical velocity as a function of time and height (mm s^{-1}) (a) over the sea 50 km from the coast, (b) near the coastline, and (c) over the land 50 km from the coast. (d) The Exner-function perturbation (labels in units of 10^{-3} J $kg^{-1}K^{-1}$, negative Exner-function perturbation areas are shaded), and (e) the horizontal velocity (labels in units of cm s^{-1}, areas with onshore-directed winds are shaded), shown as functions of time and distance from the coast at a height of 100 m.

The vertical velocities (~1–4 mm s^{-1}) that are caused by the vertical pressure gradient ($\partial w/\partial t \sim \partial \Pi'/\partial z$) can be seen to travel upward with the phase speed of sound (25 km in 75 s). After the passage of the pressure wave (acting to restore hydrostatic equilibrium) the pressure increases, causing a horizontal pressure gradient throughout the entire atmospheric column above the surface near the coast and directed towards the sea. This horizontal pressure gradient causes an acceleration in the horizontal direction ($\partial u/\partial t \sim \partial \Pi'/\partial x$, see Fig. 9(e)). This leads to divergence over the land near the coast and convergence over the sea. The divergence over the land causes the pressure to drop through the entire atmosphere ($\partial \Pi'/\partial t \sim -\partial u/\partial x$). Over the sea the pressure rises due to the convergence of the mass that diverges over land.

The horizontal velocities associated with the sound wave are very small but they are present throughout the entire atmosphere. Because the largest velocities are found near the coast, the divergence over the land and the convergence over the sea continue after the passage of the initial pressure wave. The arrival of the sound wave over the sea can be seen in Fig. 9(a). The vertical velocities at this model grid-point are much smaller than those over land, where the vertical gradients of the pressure perturbation are much larger.

The irregular pattern of the vertical velocity over land, especially after about 75 s (Figs. 9(b) and (c)), is caused by the reflection of the sound waves at temperature inversions, such as the tropopause. This is also the cause of the irregularities that can be seen in the pressure perturbation at a height of 100 m over land (Fig. 9(d)). Over the sea, where the pressure gradients and accelerations are primarily found in the horizontal direction, these reflections are not found.

The horizontal pressure gradients near the coast, caused by divergence over the land and convergence over the sea, initiate the sea breeze. The first signs of sea-breeze development can be seen near the coast in Fig. 9(e) as a deviation from the uniform wind field. The sea breeze causes convergence of mass near the coast which, in turn, causes the increasing vertical velocities in the lowest few kilometres near the coast (see Fig. 9(b)).

Figure 10 shows the Exner function perturbation as a function of height and distance from the coast after 30 s and 60 s, respectively. The movement of the acoustic wave-front can be observed by following the zero perturbation isopleth. After 30 s of heating this isopleth lies 11 km from the coast near the surface, and at a height of about 12 km above the land surface. It has a circular shape in the area between the sea surface and at a height of 12 km over land.

After 60 s of heating (Fig. 10(b)), the zero-pressure-perturbation isopleth lies 18 km from the coast at the sea surface, while over land the same contour can be found at a height of about 21 km. The Exner-function perturbation has now become negative near the surface over land, with the most negative values occurring near the coast.

Heating of the 2000 m thick layer over land disturbs the hydrostatic balance, i.e. the balance between the vertical pressure-gradient force and the buoyancy force. However, as illustrated in Fig. 11(a), there is an almost instantaneous adjustment to the hydrostatic balance because the imbalance travels away from the source region at the speed of sound (see Fig. 11(b)). Thus, sound waves act to restore the hydrostatic balance of a column of air.

The deviations behind the initial pressure wave that can be observed in Fig. 11(b) are caused by reflections of the sound waves at potential-temperature inversions, such as the tropopause, and by slight dispersion (due to the second term on the right-hand side of Eq. (5)). These results confirm those found by Bannon (1995), who investigated the reaction of a one-dimensional isothermal column of air to heating.

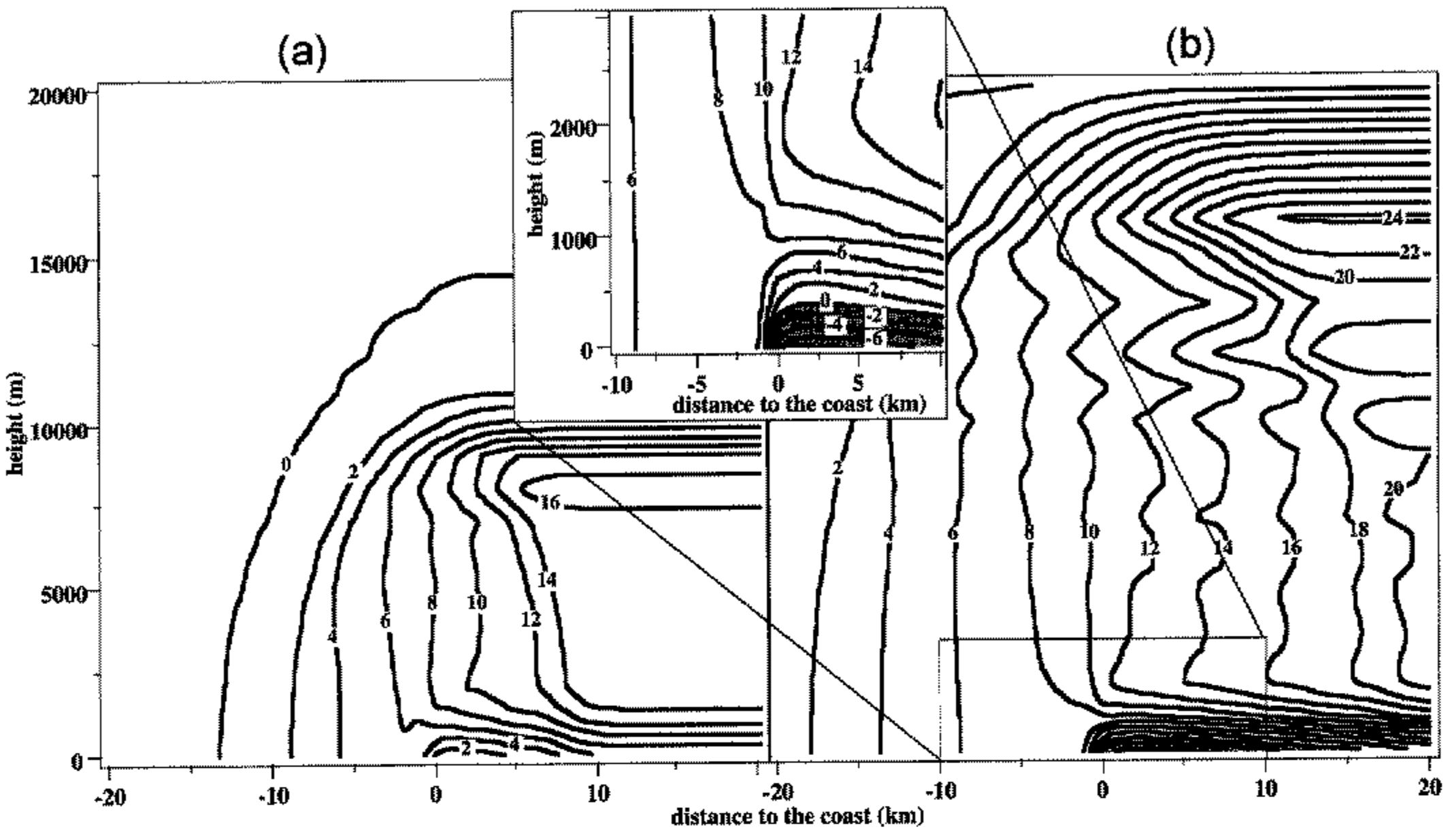

Figure 10. Exner-function perturbation (a) after 30 s, and (b) after 60 s together with an inset showing a close-up view of the area near the coast and the surface. The contours are labelled in units of 10^{-4} J kg^{-1}K^{-1}, and negative perturbations (near the surface over land) are shaded.

(*b*) *Long model run*

The reaction of the atmosphere to the heating on a much larger time- and space- scale was computed at low horizontal resolution in order to compare the simulated pressure perturbations with the observations presented in section 3 (see Figs. 2 and 3). With a horizontal grid-length of 100 km, Eqs. (1) to (4) were integrated for a period of three hours on a horizontal domain exceeding 6000 km. As expected it only takes about one hour before Π' starts changing over the sea at a distance of 1000 km from the coast (see Fig. 12(a)). The Exner-function perturbations have the same magnitude throughout the entire layer from the surface up to 5 km and above (not shown). This means that the horizontally travelling sound waves over the sea cause changes in Π' throughout the entire atmosphere.

At the coast (Fig. 12(b)) the pressure changes start immediately after the start of the heating. The vertically travelling sound waves cause Π' to become positive over the land (with Π' being zero at the surface) increasing above the surface up to 2000 m and remaining almost constant above 2000 m. The divergence induced by the horizontally travelling sound waves causes a reduction in the Exner function throughout the entire atmosphere, leading to negative values of Π' near the surface up to a height of 500 m.

Far inland (1000 km from the coast, Fig. 12(c)) Π' does not change near the surface initially, whereas it increases aloft due to the adjustment to the new hydrostatic balance. After about one hour Π' starts to decrease near the surface. This is associated with the arrival at this model grid-point of the sound waves originating near the coast, causing divergence. Again, Π' decreases in the layer from the surface up to 500 m, while Π' increases most strongly at a level of about 2000 m (the top of the heated layer).

The vertical distribution of the pressure changes compares well (qualitatively) with the interpretation by Godske *et al.* (1957) of observations made in the Alps and the Rocky Mountains. They estimated that the pressure change due to diabatic heating on a

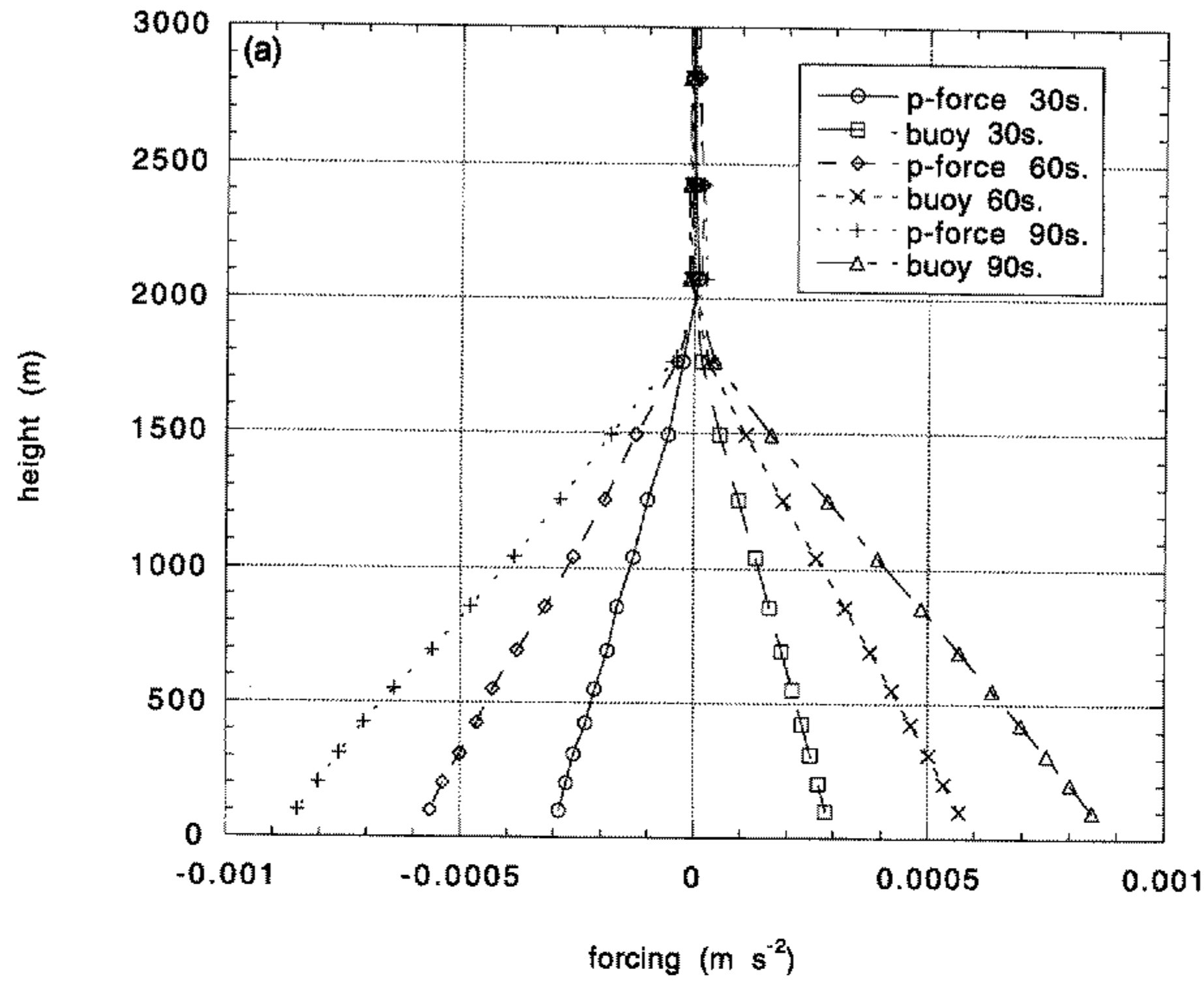

Figure 11. Profiles of the two components of the hydrostatic balance 'p-force' ($\Theta_0 \partial \Pi' / \partial z$) and 'buoy' ($g\Theta' / \Theta_0$), after 30, 60 and 90 s of heating at 30 km inland, in (a) the first 3 km and (b) the first 30 km.

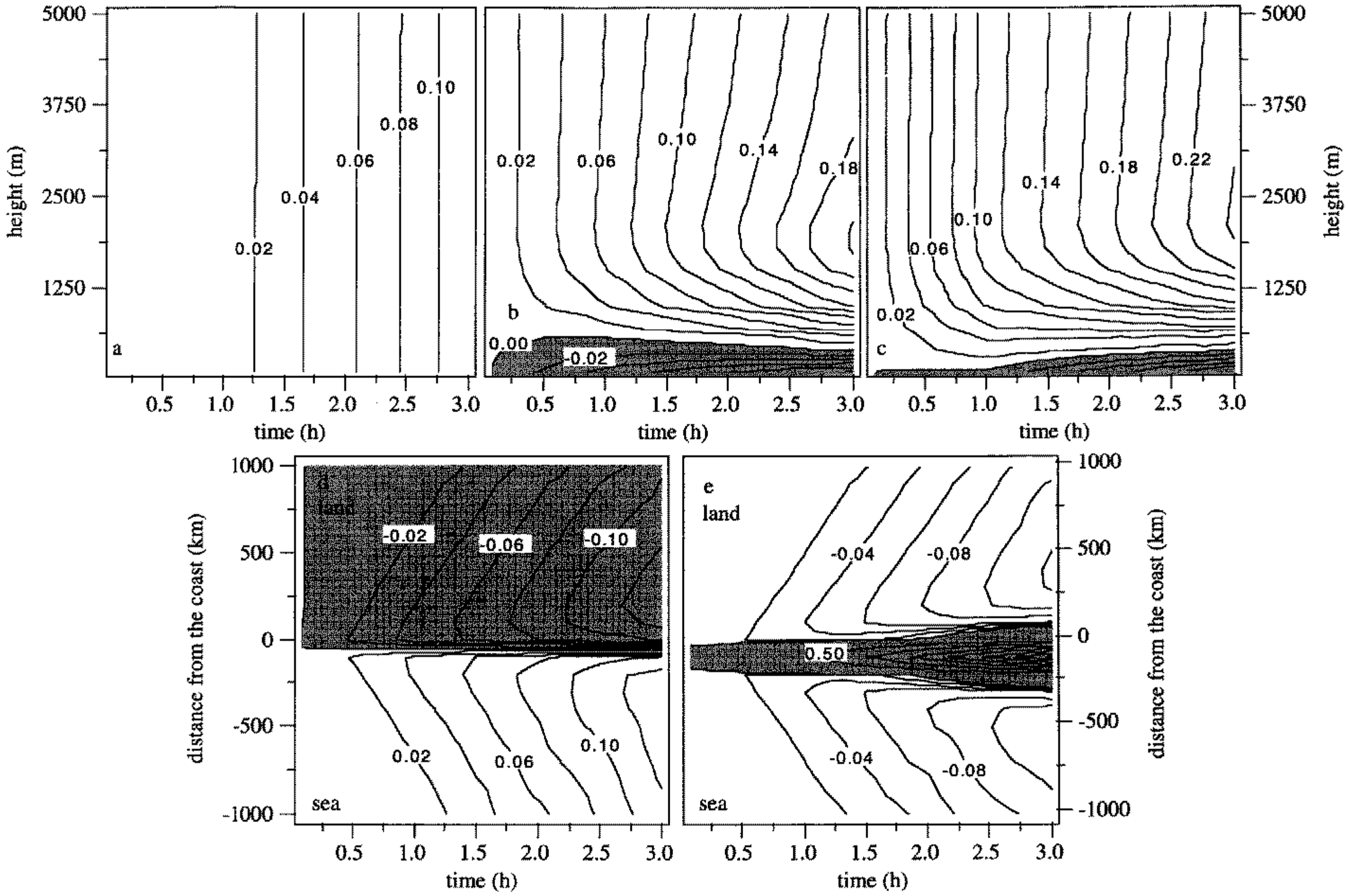

Figure 12. The Exner-function perturbation (J $kg^{-1}K^{-1}$) as a function of time and height (a) over the sea 1000 km from the coast, (b) near the coastline, and (c) over the land 1000 km from the coast. (d) The Exner-function perturbation (J $kg^{-1}K^{-1}$) and (e) the horizontal velocity (m s^{-1} with contour intervals 0.02 m s^{-1} if $u < 0$, 0.5 m s^{-1} if $u \geq 0$), shown as a function of time and distance from the coast at a height of 100 m. The shaded areas represent either negative Exner-function perturbations or onshore-directed winds.

summer day was equal to zero, on average, at a level of about 800 m above the earth's surface. According to our linear model, this height is a function of both the depth of the atmospheric layer that is heated diabatically, and the dimensions of the land mass that is heated.

In Fig. 12(d) it can be seen that Π' has the same magnitude over the land as over the sea near the surface, but with the opposite sign. The difference in the rate of change of the Exner function near the surface between the model grid-points over the land and over the sea is about 0.1 J $K^{-1}kg^{-1}h^{-1}$, which corresponds to a rate change of pressure of about 0.35 hPa h^{-1}. The imposed average diabatic heating (0.5 K h^{-1}) of the layer from the earth's surface to a height of 2000 m corresponds to a surface sensible-heat flux of 275 W m^{-2}. The average maximum surface sensible-heat flux for the 53 cases of sea breezes described in section 3 is estimated to lie between 150 and 200 W m^{-2}. This means that the simulated difference in surface-pressure change between the land and sea compares well with the observed maximum value at 11 UTC of about 0.25 hPa h^{-1} (Fig. 7).

There is a seaward directed wind in a large part of the model domain (Fig. 12(e)). The divergence over the land and the convergence over the sea continue at a constant rate due to the constant gradients in the horizontal wind component. Near the coast the pressure gradients induced near the surface by divergence over the land and convergence over the sea (see Fig. 12(d)) cause the initiation of the sea breeze. The onset of the sea breeze near the coast can be seen very clearly in Fig. 12(e). In three hours the sea breeze reaches a maximum, with an onshore wind component of 3.5 m s^{-1}. Of course, by this time the validity of the linearization has broken down.

The horizontal velocities associated with the horizontal expansion of the air over land are of the order 0.1 m s^{-1}; this is very difficult to observe from observations. The maximum vertical velocity is even smaller ($\sim$ mm s^{-1}). Because the observations used in this study have a temporal resolution of one hour and extend over a distance of about 400 km, it is very difficult to find explicit evidence of pressure waves travelling with the speed of sound. To be able to find any evidence of this effect in surface-pressure observations, one would have to look at variations in the north–south direction over a large continent (because the time of sunrise has to be uniform).

Nevertheless, there is *implicit* evidence of sound waves because several characteristic features of the pressure distribution associated with acoustic waves induced by the diabatic heating are consistent with the, as yet unexplained, observations compiled by Godske *et al.* (1957) and Simpson (1994) displayed in Figs. 2 and 3.

Buoyancy waves are not observed in the numerical experiments described above. This is due to the fact that the period of these waves is longer than the length of the integration. The period of the buoyancy waves is given by (see also Eq. (6)):

$$\omega^2 = \frac{\alpha^2 N^2}{\alpha^2 + \gamma^2} = \frac{N^2}{1 + \left(L^2/H^2\right)}, \tag{7}$$

where L is the horizontal wavelength and H is the vertical wavelength (2000 m in this case). In the integration with a 5 km grid-length, the wavelength, L, of the buoyancy waves is more than 10 km. With $N = 10^{-2}$ s^{-1}, the maximum frequency of buoyancy waves is 2×10^{-3} s^{-1} and the associated period about 52 min; this is much longer than the 200 s of integration. In the integration with a 100 km grid-length, the wavelength, L, of the buoyancy waves is more than 200 km. With $N = 10^{-2}$ s^{-1}, the maximum frequency of the buoyancy waves is 10^{-4} s^{-1}. This corresponds to a minimum period of approximately 17 hours, which is much longer than the 3 h extent of the integration.

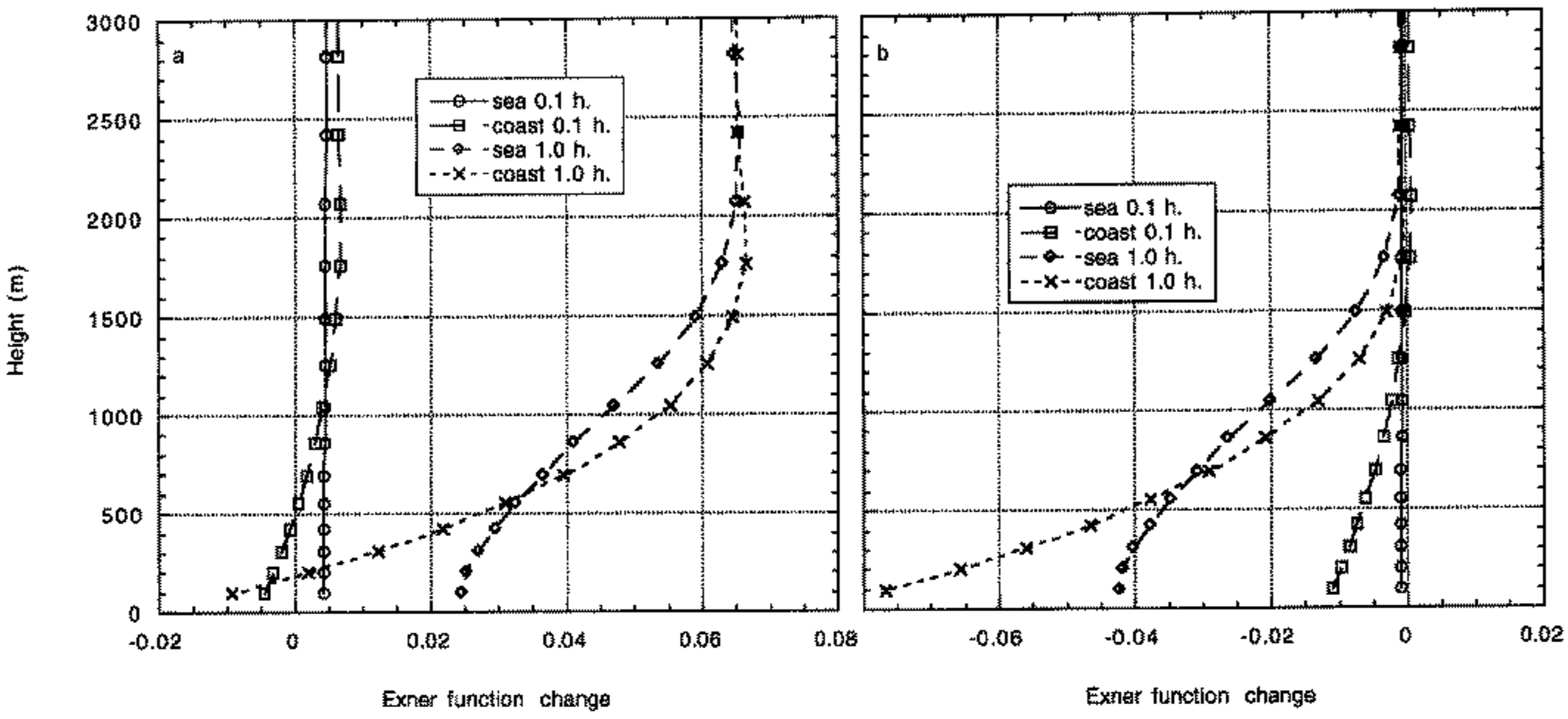

Figure 13. The Exner-function perturbation (J $kg^{-1}K^{-1}$) as a function of height at the coast and 10 km out at sea for (a) the non-hydrostatic run, and (b) the hydrostatic run.

Increasing the integration time of both experiments clearly shows the development of buoyancy waves. However, these results cannot be presented here, as the model we use is linear and the linear assumption breaks down for these longer integrations.

(c) *Implications for hydrostatic modelling of sea breezes*

In order to find if the results of the previous sections have implications for the modelling of sea breezes we have compared the non-hydrostatic model with a hydrostatic version of the model described above. The hydrostatic version of the model was obtained by altering Eqs. (2) and (4). In the hydrostatic model Eq. (2) becomes:

$$\frac{\partial u}{\partial x} + \frac{\partial w}{\partial z} = 0. \tag{8}$$

w is calculated from Eq. (8), while Π' is calculated by integrating the hydrostatic equation downwards from the model top, assuming a constant pressure as the top boundary condition:

$$\Theta_0 \frac{\partial \Pi'}{\partial z} = g \frac{\Theta'}{\Theta_0}. \tag{9}$$

We have made one-hour model runs with the hydrostatic and the non-hydrostatic versions of the model on a grid with a horizontal grid-length of 10 km. The forcing function and the initial profiles are the same as in the previous runs. The most notable difference between the two cases is that the pressure rises throughout almost the entire atmosphere for the non-hydrostatic case, whereas it remains at its initial value above the warming layer in the hydrostatic case (Figs. 13(a) and (b)).

However, it is particularly notable in Fig. 14 that the horizontal pressure gradient is about the same for the hydrostatic run as for the non-hydrostatic run. The hydrostatic pressure gradient is slightly larger in the sea-breeze layer yielding a somewhat stronger sea breeze (10%). In the return-current layer (from 600 to 2000 m), the non-hydrostatic pressure gradient is larger, resulting in a stronger return current (20%). The weaker sea breeze, together with the stronger return current, in the non-hydrostatic case is caused, in part, by the sea-breeze-opposing flow and by the return-current-strengthening flow

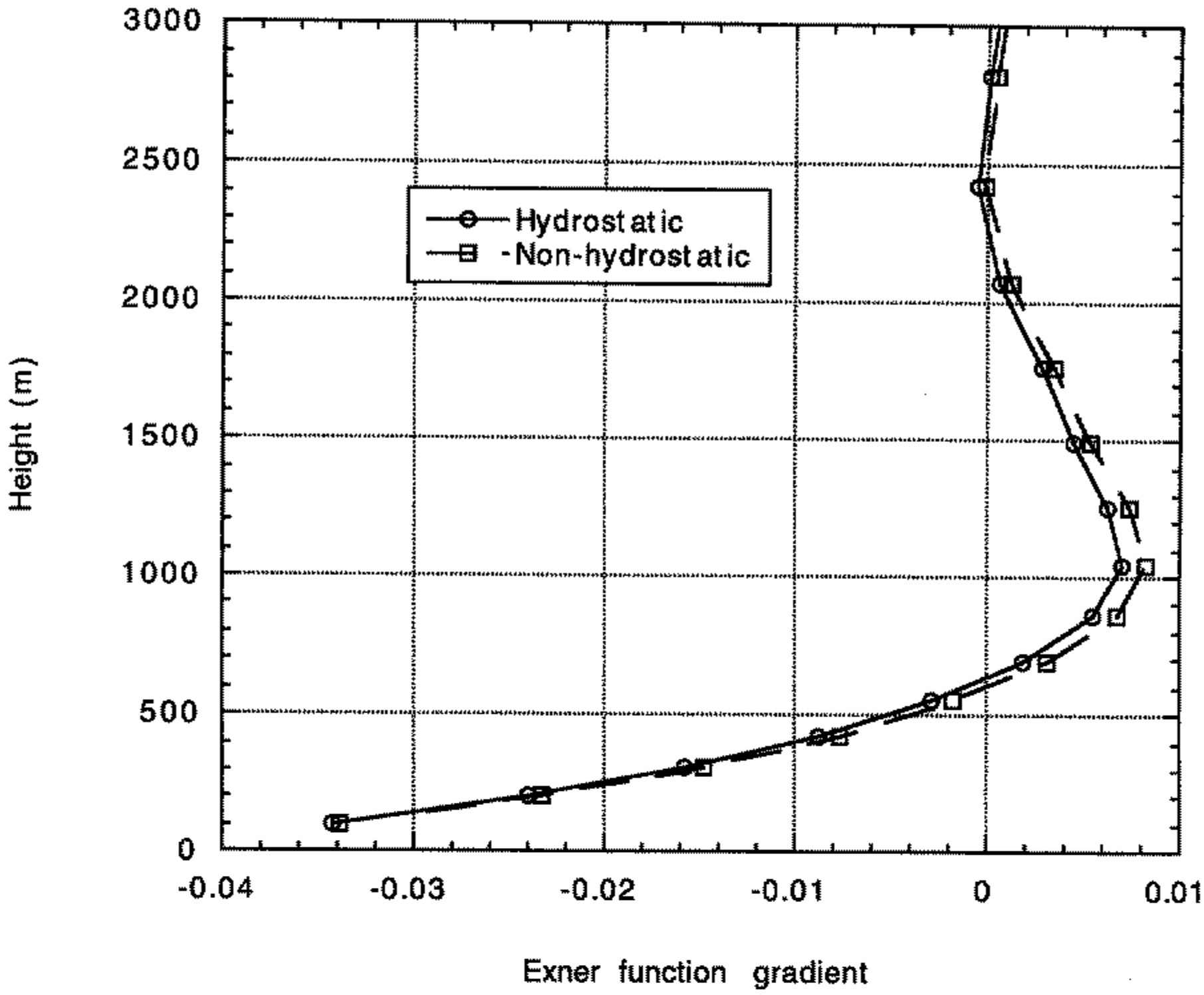

Figure 14. Comparison of the horizontal Exner-function gradient (J $kg^{-1}K^{-1}(10\ km)^{-1}$) as a function of height near the coast after one hour for the non-hydrostatic run and the hydrostatic run.

of diverging air from the land due to horizontal expansion, an effect neglected in the hydrostatic model.

5. Conclusions

This paper describes an attempt, using observations and a linear model, to evaluate the validity of three 'hydrostatic' explanations of sea-breeze initiation found in well-known basic meteorological textbooks. The most proclaimed explanation is called the upward theory. It predicts a decrease of the surface pressure in a limited area (due to the vertical expansion of diabatically heated air over land and the associated mass divergence aloft towards the sea). However, this is not in fact observed. From the analysis of observations at an array of ten stations located at sea up to 200 km from the coast and inland to about 150 km, it appears that the decrease in surface pressure over land on a typical sea-breeze day, relative to the average change in surface pressure at all 10 stations, is in fact strongest *far from the coast*.

All three hydrostatic explanations of sea breezes neglect the actual process of hydrostatic adjustment, which is accompanied by sound-wave propagation (see also Bannon (1995)). From the numerical experiments it appears that this process needs to be taken into account in order to understand the development of the pressure gradients that initiate the sea breeze. Sound waves are generated over land when the air expands due to diabatic heating. Vertically travelling sound waves induce a pressure increase *through the entire atmosphere above the heated layer within a few minutes*. Horizontally travelling sound waves induce a surface-pressure decrease over the land and a surface-pressure increase over the sea, with the resulting pressure gradient initiating the sea

breeze. The surface-pressure decrease over land is observed first at the coast, but the signal travels inland at the speed of sound (about 300 m s^{-1}). So, within an hour, points at a distance of more than 1000 km from the coast experience a surface-pressure decrease.

The pressure decrease near the earth's surface over land, as well as the pressure increase aloft, is in accord with the observations at mountain stations compiled by Godske *et al.* (1957) and with the analysis by Simpson (1994) of observed daytime surface-pressure changes in summer over the European continent and the adjacent seas. The horizontal velocities connected with the sound waves are about 0.1 m s^{-1} after 3 h of heating. The vertical velocities are about 1 mm s^{-1}. Unfortunately these velocities are probably too small to be retrieved from observational data.

Because the so-called *level of no pressure change* depends on the thickness of the heated layer (which, in turn, may depend on the flow) we are confronted with a serious problem in the specification of an upper or lower boundary condition for the pressure in hydrostatic sea-breeze models. In most sea-breeze models, the pressure at the top of the domain is assumed constant. The pressure below is computed by integrating the hydrostatic relation downwards. This assumption was introduced in the linear model used in this study and the solution was compared with the full linear model. From this comparison it appears that after one hour the hydrostatic sea breeze is 10% stronger than the non-hydrostatic sea breeze, while the hydrostatic return current is about 20% weaker. These differences are caused by slightly different pressure gradients and by the sea-breeze-opposing velocity field associated with expansion, a process *neglected* in the hydrostatic model.

ACKNOWLEDGEMENTS

We would like to thank Bert Holtslag, Peter Duynkerke and the turbulence discussion group of IMAU/KNMI for the useful comments on earlier versions of this paper.

REFERENCES

Anthes, R. A. and Warner, T. T. 1974 Development of hydrodynamic models suitable for air pollution and other mesometeorological studies. *Mon. Weather Rev.*, **106,** 1045–1078

Atkinson, B. W. 1981 *Meso-scale atmospheric circulations.* Academic press, London

Bannon, P. R. 1995 Hydrostatic adjustment: Lamb's problem. *J. Atmos. Sci.*, **52,** 1743–1752

Brunt, D. 1939 *Physical and dynamical meteorology.* Cambridge University Press, Cambridge

Bjerknes, V., Bjerknes, J., Solberg, H. and Bergeron, T. 1933 *Physikalische hydrodynamik.* Berlin Verlag von Julius Springer

Chapman, S. and Lindzen, R. S. 1957 *Atmospheric tides.* D. Reidel Publishing Company, Dordrecht

Defant, F. 1951 Local winds. *Compendium of meteorology.* American Meteorological Society

Estoque, M. A. 1962 The sea breeze as a function of the prevailing synoptic situation. *J. Atmos. Sci.*, **19,** 244–250

Godske, C. L., Bergeron, T., Bjerknes, J. and Bundgaard, R. C. 1957 *Dynamic meteorology and weather forecasting.* Carnegie Institution and American Meteorological Society, Washington and Boston

Hess, S. L. 1959 *Introduction to theoretical meteorology.* Henry Holt and Company, New York

Holton, J. R. 1992 *An introduction to dynamic meteorology.* Academic Press, San Diego

Koschmieder, H. 1933 *Dynamische Meteorologie.* Academische Verlagsgesellshaft, Leipzig

Nicholls, M. E. and Pielke, R. A. 1994a Thermal compression waves. I: Total energy transfer. *Q. J. R. Meteorol. Soc.*, **120,** 305–332

Nicholls, M. E. and Pielke, R. A. 1994b Thermal compression waves. II: Mass adjustment and vertical transfer of total energy. *Q. J. R. Meteorol. Soc.*, **120,** 333–359

Physick, W. L. 1976 A numerical model of the sea breeze phenomenon over a lake or gulf. *J. Atmos. Sci.*, **33,** 2107–2135

Pielke, R. A. 1974 A three-dimensional numerical model of the sea breezes over South Florida. *Mon. Weather Rev.*, **102,** 115–139

1984 *Mesoscale meteorological modeling.* Academic Press, Orlando

Scorer, R. S. 1997 *Dynamics of meteorology and climate.* John Wiley and Sons, Chichester

Simpson, J. E. 1994 *Sea breeze and local wind.*, Cambridge University Press

Tijm, A. B. C., Holtslag, A. A. M. and Van Delden, A. J. 1999 Observations and modelling of the sea breeze with the return current. *Mon. Weather Rev.*, **127,** 625–640

US Government Printing Office 1976 *US Standard Atmosphere, 1976.* Government Printing Office, USA

Van Delden, A. J. 1992 The dynamics of meso-scale atmospheric circulations. *Phys. Rep.*, **211,** 251–376

Von Hann, J. 1899 Täglicher Gang des Barometers auf Pikes Peak (4308 m) und zu Colorado Springs (1856 m). *Meteorol. Zeit.*, **16,** 87–91

Wagner, A. 1932 Der tägliche Luftdruck- und Temperaturgang in der freien Atmosphäre und in Gebirgstälern. *Gerlands Beitr. Geophys.*, **37,** 315–344

Willett, H. C. and Sanders, F. 1959 *Descriptive meteorology.* Academic Press, New York